Ab initio quantum chemical investigation of arsenic sulfide molecular diversity

Atsushi Kyono[1]*

[1]Div. of Earth Evolution Sci., Grad. Sch. of Life & Environmental Sci., Univ. of Tsukuba

The structural diversity of arsenic sulfide molecules in compositions between As_4S_6 and As_4S was investigated using ab initio quantum chemical calculations. The As_4S_6 molecule consists of four trigonal pyramid coordinations of As atoms bonding to three S atoms. In the As_4S_5 composition, only one type of molecular configuration corresponds to an uzonite-type molecule. In the As_4S_4 composition, two molecular configurations exist with realgar-type and pararealgar-type molecules. Three molecular configurations are in the As_4S_3 composition. The first configuration comprises trigonal pyramidal As atom coordinations of two types: bonding to two S atoms and one As atom, and bonding to one S atom and two As atoms. The second is the molecular configuration of dimorphite. The third comprises trigonal pyramidal As atom coordinations of two types: bonding to three As atoms, and bonding to one As atom and two S atoms. The As_4S_2 composition allows molecular configurations of two types. One is comprised of trigonal pyramidal As atom configurations of one type bonding to two As atoms and one S atom. The other comprises trigonal pyramidal As atom coordinations of three types: bonding to two S atoms and one As atoms, bonding to one S atom and two As atoms, and bonding to three As atoms. The As_4S molecule has trigonal pyramidal As atom coordinations of two types: bonding one S atom and two As atoms, and bonding to three As atoms. The As_4S composition permits only one molecular configuration, which suggests that the mineral duranusite comprises the As_4S molecular geometry. In all, ten molecular configurations are predicted in the molecular hierarchy of the arsenic sulfide binary system. The simulated Raman spectral profiles are helpful in searching for undiscovered arsenic sulfide minerals.

Keywords: arsenic sulfide minerals, molecular configuration, diversity, hierarchy, ab initio quantum chemical calculation

SMP44-P02   Room:Convention Hall   Time:May 20 18:15-19:30

Volume and crystal structure change due to He incorporation into cristobalite at high pressures

Masanori Matsui[1]*, Tomoko Sato[2], Nobumasa Funamori[3]

[1]School of Sci., Univ. of Hyogo, [2]Dept. of Earth and Planetary Systems Sci., Hiroshima Univ., [3]Dept. of Earth and Planetary Sci., Univ. of Tokyo

Based on powder X-ray diffraction measurements under high pressures and room temperature at Photon Factory, Tsukuba, Sato et al.(2012) have recently found unique behavior of cristibalite in helium pressure medium in a diamond anvil cell, where, on compression, cristobalite II transformes to a new phase (called cristobalite-He I) at about 8 GPa, then on subsequent decompression from about 15 GPa, cristobalite-He I transforms to another new phase (called cristobalite-He II) at about 7 GPa. They tentatively assigned cristobalite-He I and II to have orthorhombic and rhombohedral lattices with molar volumes greater than about 30 % and 25 % larger than cristobalite, respectively. Here we use first-principle calculations to study structural and enegetic properties of cristobalite-He I and II in more detail.

All calculations were performed with the ab initio simulation package VASP (Kresse and Furthmuller, 1996). The projector-augmented wave (PAW) method (Blochl, 1994) was used in the generalized-gradient approximation (GGA) for the exchange-correlation functional (Perdew et al., 1996). Atomic positions were relaxed with observed or hypothetical crystal-symmetry constraints. In order to check the reliability and applicability of the computations, we first calculated the structures and energies of cristobalite and cristobalite II, with the results that the calculated values reproduce the observed ones (Dove et al., 2000; Dera et al., 2011) accurately.

Cristobalite transforms to cristobalite II at 1.5 GPa and room temperature (Palmer and Finger, 1994; Dove et al., 2000). The initial lattice parameters and atomic positions of both Si and O were taken from cristobalite II (Dove et al., 2000; Dera et al., 2011), while the He positions were taken to be situated in large voids in cristobalite II. We tested several structural models for both cristobalite-He I and II, and finally found enthaly-minimized models that reproduces the measured X-ray diffraction patterns of the two phases (Sato et al., 2011), respectively, accurately.

Keywords: cristobalite, helium, high pressure, crystal structure, phase transition

SMP44-P03 　　　　　 Room:Convention Hall 　　　　　 Time:May 20 18:15-19:30

Stability of Orthopyroxene in pyroxene quadrilateral at 1 atm and High Temperatures

Shugo Ohi[1]*

[1]Graduate School of Science, Kyoto University

Pyroxene is one of the most important rock-forming minerals not only for its abundant occurrence but also for various paragenesis which provide information on the thermal history of pyroxene-baring rocks. In the system $Mg_2Si_2O_6$ (En) -$CaMgSi_2O_6$ (Di), there had been the controversy about the appearance and stability of the orthopyroxene (Opx) phase near 1400 C other than protopyroxene (Ppx) since the discovery by Foster and Lin (1975). In recent years, Ohi et al. (2008) observed the phase transition between low-temperature Opx (LT-Opx) and high-temoperature Opx (HT-Opx) at 1170 C during both heating and cooling processes by high-temperature synchrotron X-ray powder diffraction experiments for the composition of $(Ca_{0.06}Mg_{1.94})Si_2O_6$. They concluded that Opx the phase near 1400 C was HT-Opx and that below 1000 C was LT-Opx. In $Mg_2Si_2O_6$-$CaMgSi_2O_6$-$CaFeSi_2O_6$-$Fe_2Si_2O_6$ system, Opx contain a little amount of Ca and have the composition between $Mg_2Si_2O_6$-$Fe_2Si_2O_6$ solid solution. However, there was no report about the stability field of HT-Opx in pyroxene quadrilateral system. Purpose in present study is to reveal the stability field of LT- and HT-Opx in pyroxene quadrilateral system by sythesis experiments.

About 20 smples were synthesized from gels with 6 kinds of composition in the range of Ca : Mg : Fe = 0.03-0.15 : 0.92-0.65 : 0.05-0.20 at 1180, 1280, 1345 and 1375 C. Run durations were about 3-14 days. All samples were synthesized dry at 1 atm using a H_2 + CO_2 gas mixture to maintain the oxygen fugacity near that of the iron-wustite assemblage. They were analyzed with X-ray powder diffractometer (XRD: RIGAKU, SmartLab), a scanning electron microscope (SEM: HITACHI S-3000H) + energy dispersive X-ray spectrometer (EDX: HORIBA EMAX7000) and an electron backscattered diffraction (EBSD: HKL, CHANNEL5). Peaks of clinoenstatite (Cen: inverted from protoenstatite) and pigeonite (Pig) were not identified by XRD in present study. Therefore, these phases were described as Ca-poor Cpx.

At 1180 C, most crystals were smaller than 5 um in diameter and the chemical compositions of those could not be analyzed method by SEM-EDX. All XRD patterns of crystals synthesized at 1180 C showed the presence of Ca-poor Cpx and (or) Di and there were no Opx peaks in XRD spectra. At 1280 C, most crystals were about 3-5 um in diameter and some crystals were large enough to be analyzed by SEM-EDX. Analytical data by SEM-EDX showed the presence of Opx ($Ca_{0.06}Mg_{1.84}Fe_{0.10}Si_2O_6$). XRD patterns showed the presence of Opx in the samples with chemical compositions of Fs/(En + Fs) > 0.1, whereas there were no Opx in the sample Fs/(En + Fs) < 0.1. At 1345 and 1375 C, most crystals were about 5-10 um in diametere. Analytical data by SEM-EDX and SEM-EBSD showed the presence of Cen, Opx, Pig and Di.

In Fe-free En-Di system at 1 atm, the stability field of LT-Opx is below 1005 C and that of HT-Opx is above 1370 C. In present study, there were Opx in some samples synthesized above 1280 C whereas there were no OPx in samples synthesized at 1180C. It suggested that all Opx in present study were HT-Opx and the stability field of HT-Opx was spread to lower temperature with increasing Fe-content in HT-Opx. This trend was same as the stability field of Pig.

Keywords: orthopyroxene, high temperature, enstatite-diopside-hedenbergite-ferrosilite system, phase transition

Thermal equation of state of manganite

Akio Suzuki[1]*

[1]Tohoku University

Manganese(III) oxide hydroxide is found in nature as the minerals groutite (alpha-MnOOH), feitknechtite (beta-MnOOH), and manganite (gamma-MnOOH). Manganite is one of the naturally occurring polymorphs of Mn3+OOH with an InOOH-related structure. The oxide hydroxides of trivalent cations have an InOOH-related structure, in which the trivalent cation is octahedrally coordinated by oxygen. InOOH, beta-CrOOH, epsilon-FeOOH, and delta-AlOOH have orthorhombic unit cells. However, manganite is monoclinic because of the Jahn?Teller distortion. Here we report the pressure?volume-temperature relation of gamma-MnOOH. The aim of this study was to determine the compression behavior of an oxide hydroxide with an InOOH-related structure.

The high-pressure X-ray diffraction study was carried out at the station NE7A at the Photon Factory Advanced Ring (PF-AR) in High Energy Acceleration Research Organization (KEK). The PF-AR operates at 6.5 GeV with an injection current of 60 mA. We used a Kawai-type multianvil apparatus driven by a large volume press, MAX-III. Tungsten carbide cubes (Tungaloy grade F) of 22 mm edge length were used for high-pressure generation.

Experiments were performed up to a pressure of 18.0 GPa and a temperature of 700K. The pressure?volume data were fitted by a third-order Birch?Murnaghan equation of state with the following parameters: V_0 = 135.22(8) A^3, K_0 = 77(2) GPa and K_{0T} = 12.0(5). The temperature dependence of the bulk modulus was determined to be dK/dT= -0.022(6) GPa/K. This study shows that the most compressible axis is the b-axis. The beta angle in the monoclinic unit cell decreases with increasing pressure.

Keywords: X-ray diffraction, Equation of state, High pressure, MnOOH, Synchrotron radiation, Hydrous mineral

Thermal expansivities of stishovite and akimotoite by high-pressure Raman and high-temperature X-ray diffraction methods

Monami Yamazaki[1]*, Hiroshi Kojitani[1], Masaki Akaogi[1]

[1]Dept. Cemistry, Gakushuin Univ

High-pressure high-temperature experiments suggest that SiO_2 stishovite and $MgSiO_3$ akimotoite are constituents of subducted oceanic plate and continental crust. Because they are unstable at 1 atm and at high temperatures, it is difficult to directly measure their thermal expansivities. Therefore, they have been poorly constrained. In this study, we have determined thermal expansivities of SiO_2 stishovite and $MgSiO_3$ akimotoite by theoretical calculation based on high-pressure Raman spectroscopic data and high-temperature X-ray diffraction measurements.

High-pressure Raman spectroscopy was performed in a pressure range from 1 atm to 10 GPa using a diamond anvil cell and a micro-Raman spectrometer. SiO_2 stishovite and $MgSiO_3$ akimotoite samples were synthesized at high pressure and high temperature. The thermal Gruneisen parameters were obtained from weighted average of the mode-Gruneisen parameters which were determined from pressure shifts of Raman peaks. Thermal expansivities were calculated from the Gruneisen equation. The heat capacities at constant volume (C_V) were calculated using lattice vibrational model. High-temperature X-ray diffraction measurements of $MgSiO_3$ akimotoite were performed in a temperature range of 293.8 - 773 K. The thermal expansivity was determined from the temperature dependence of the unit cell volume.

Obtained thermal expansivities were expressed using the polynomial of temperature: alpha = a + bT + cT^{-1} + dT^{-2} The coefficients for SiO_2 stishovite and $MgSiO_3$ akimotoite were determined to be a = 1.85E-5, b = 3.25E-9, c = -2.41E-3, d = -1.11E-1, and a = 2.53E-5, b = 7.62E-9, c = -8.63E-4, d = -5.51E-1, respectively.

The thermal expansivity of SiO_2 stishovite in this study is smaller than that obtained from high-pressure high-temperature in situ XRD measurements by Nishihara et al. (2005), and agrees with that obtained from optimization of thermodynamic data assessment by Mao et al. (2001). The heat capacity at constant pressure (C_P) calculated using the thermal expansivity by Nishihara et al. (2005) is 5 % larger than that measured by thermal relaxation method by Akaogi et al. (2011). On the other hand, C_P calculated using the thermar expansivity of this study shows good agreement with Akaogi et al. (2011). Therefore, our thermal expansivity of stishovite is internally consistent with the measured heat capacity data.

Our thermal expansivity of $MgSiO_3$ akimotoite derived by the theoretical method is closer to those determined by high-temperature XRD measurements in this study and Ashida et al. (1988) rather than that of Wang et al. (2004) obtained from high-pressure high-temperature in situ XRD measurements. This result suggests that the thermal expansivity of $MgSiO_3$ akimotoite is larger than previously reported values.

Keywords: akimotoite, stishovite, thermal expansivities, high-pressure Raman spectroscopy, high-temperature X-ray diffraction measurements

The synthetic opal fixed in hydrothermal environment

Yuko Yamasaki[1]*, Hiroshi Isobe[1]

[1]Grad. Sch. Sci. Tech., Kumamoto Univ

Opal shows a characteristic opalescence by periodic stacking of amorphous silica spherules with several hundred nanometers in diameter. The amorphous silica spherules can be synthesized by the Stoeber method with hydrolysis of tetra ethyl orthosilicate (TEOS) solution. The initial silica spherules are dispersed in suspension. In this study, we report stable synthetic opal with opalescence domains fixed in hydrothermal conditions.

The silica spherule suspension made by the Stoeber method is concentrated and poured in silica glass test tube with 6mm in inner diameter and approximately 30mm in height. The silica test tubes are sealed in teflon crucibles or microreacters with distilled water and heated to 100 degrees Celsius - 250 degrees Celsius for 1 to 75 days. Depth of distilled water outside the silica glass test tubes does not exceed the height of the test tube. After the run durations, surface of the settled silica is covered with resin and cut to observe vertical section by optical and electron microscopes.

In the run products of 100 degree C to 200 degree C, we can see opalescence domains up to mm scale. Especially, in the run products of 200 degree C, we can see development of opalescence domains with various colors. Under the electron microscopy, deformation of silica spherules or cementation is observed in run products with opalescence. The hydrothermal environment can play essential role to form opalescence domains and fixation from amorphous silica spherule suspension.

Keywords: opal, hydrothermal synthesis, opalescence domain, amorphous silica

SMP44-P07   Room:Convention Hall   Time:May 20 18:15-19:30

Activation of hole charge carriers and generation of electromotive force in gabbro blocks induced by non-uniform loading

Akihiro Takeuchi[1]*, Toshiyasu Nagao[1]

[1]Earthq. Predict. Res. Cent., Inst. Ocenic Res. Dev., Tokai Univ.

When one end of vacuum-dried gabbro blocks was subjected to uniaxial loading, the unloaded end became electronically positive (+80 mV at 50-MPa). Hot point probe tests using the hot-probe with 423 K of the temperature and the cold one with 293 K found that the Seebeck coefficient of the loaded volume decreased from ~15.8 mV/K to ~14.9 mV/K when loaded, while the coefficient of the unloaded end did not change remarkably (~15.6 mV/K). This means that this gabbro originally included a small number of hole charge carriers and the carriers in the loaded volume increased when loaded. From the viewpoint of the fundamental band model of solid state, the most reasonable mechanism of the increment is the decrease of the energy gap between the acceptors and the valence band top. Shear stress/strain would effectively shift the energy levels because early studies have found that the electronic conductivity of gabbro is almost independent of the hydrostatic pressure. Based on this idea, a generation model of the stress-induced electromotive force is proposed. Since this model is expected to be universally applicable to various types of rocks, similar electromotive forces in the crustal scale may be induced by seismic, volcanic, and tidal activities in the Earth and Moon.

Keywords: gabbro, hole charge carrier, electromotive force, Seebeck coefficient

Ferrous to ferric ratio measurement in chlorite using electron energy-loss spectroscopy (EELS)

Sayako Inoue[1]*, KASAMA, Takeshi[2], Kogure, Toshihiro[1]

[1]Earth & Planetary Sci., Univ. Tokyo, [2]Center for Electron Nanoscopy, DTU

Determination of Fe^{3+}/Fe_{total} ratio in iron-bearing minerals is important and has been conducted using several analytical techniques such as Mosbauer spectroscopy, X-ray absorption near-edge structure (XANES) and X-ray photoelectron spectroscopy. Compared to these techniques, electron energy-loss spectroscopy (EELS) in Transmission electron microscopy (TEM) is capable of giving information of the chemical state of constituting elements in specimens, with a spatial resolution down to the nanometer scale. Detailed analysis of energy-loss near-edge structure (ELNES) of $Fe-L_{2,3}$ core-loss edges provides information about the iron oxidation state, and several methods have been proposed to quantify Fe^{3+}/Fe_{total} from the ELNES of iron (Garvie and Buseck, 1998; van Aken et al., 1998). However, because a number of silicate minerals are electron-beam sensitive, the influence of radiation damage on the quantification of Fe^{3+}/Fe_{total} by EELS should be considered. Moreover, sample preparation processes for TEM such as argon ion-milling and focused-ion-beam (FIB) milling form a damage layer on the specimen surface, which may also affect the quantification. In this study Fe^{3+}/Fe_{total} quantification in chlorite, rather beam-sensitive iron-bearing phyllosilicates, has been performed using EELS equipped to a field-emission gun TEM with a monochromator, considering the influence of radiation damage and sample conditions on the measurement.

Fe^{3+}/Fe_{total} ratios obtained from the same grain of chlorite indicated that the ratio increases significantly with the electron dose to be radiated during TEM observation and EELS acquisition, suggesting that the oxidation of iron proceeds with vitrification of chlorite by radiation. Hence, it was necessary to acquire several Fe^{3+}/Fe_{total} ratios as a function of electron dose (i.e., time) and estimate 'the damage-free ratio' by extrapolation. The surface damage layers with a thickness of several tens of nanometers, which were formed during FIB milling, are likely oxidized and therefore partially associated with the increase in the Fe^{3+}/Fe_{total} ratios.

Keywords: EELS, TEM, Phyllosilicate, Chlorite, Iron valence state, FIB

SMP44-P09   Room:Convention Hall   Time:May 20 18:15-19:30

Change in fayalites with ultraviolet rays and water

Nobuo Komori[1]*

[1]Ota ward Kamata junior high school

I have been doing an experimental research of weathering on rocks by ultraviolet rays and waters in a junior high school science club since 2002. This time,it aimed to see the reaction of fayalite when it is soaked in distilled water and irradiated with ultraviolet rays.

It is said that there is much basalt that perhaps contains fayalite on Mars surface. Moreover,it is estimated that there was water on Mars surface in the past. Therefore,I think that ultraviolet rays and water are one of the factors which change rocks on Mars surface.

In this research, fayalites, which total weight is about 10g, are put in the test tube filled with distilled water. The diameter of these fayalites is about 3mm~5mm.They are grain shaped and the color is darkgreen. The test tube is irradiated with ultraviolet rays with their peak wave length of 254 nm. Another experiment was done as a comparison under the same condition but without ultraviolet. The tubes were irradiated with ultraviolet rays for three months. The illuminance of ultraviolet rays is $40w/m^2$ when the experiments were first strated.

As a result of this experiment,a lot of light brown powder was generated in both of the test tubes that were irradiated with ultraviolet rays. However, the tube without ultraviolet rays irradiation generated less powder. Therefore, we can conclude that irradiation of ultraviolet rays causes larger amount of the powder. From the result of EPMA analysis, the powder is the amorphous iron oxide hydroxide.

There are many fresh structures that is like hole about 10micron m on uv iraadiated fayalite.

But there are few these structures on uv not iraadiated fayalite.

Moreover, we can estimate that ultraviolet rays might promote the change of fayalites in the water. It is presumed that water existed in the past on Mars surface.

I think that there is a possibility on the Mars surface that the rocks contained fayalites were oxidized by the water and ultraviolet rays.

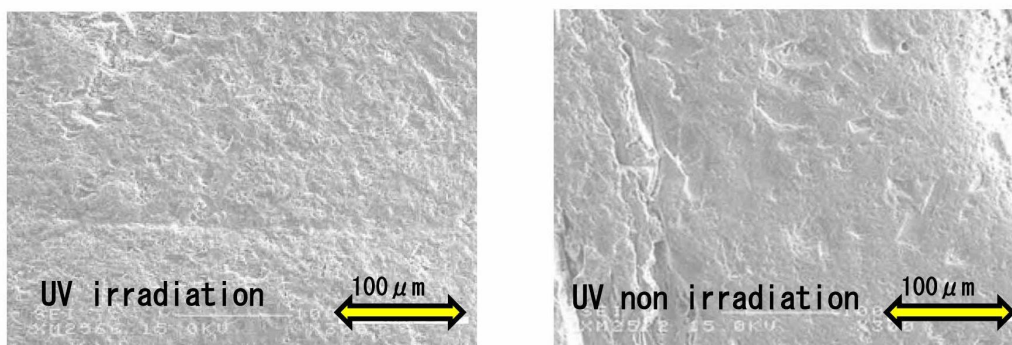Keywords: ultraviolet rays, water, fayalite,, iron(III) oxide, change, Mars

Fig. SEM images of the surfaces of fayalite specimens soaked in distilled water for 3 months with and without UV irradiation.

Annealing and radiation effects on cathodoluminescence of zircon

Yuta Tsuchiya[1*], Masahiro Kayama[2], Hirotsugu Nishido[1], Yousuke Noumi[1]

[1]Department of Biosphere-Geosphere Science, [2]Department of Earth and Planetary Systems Science

Cathodoluminescence (CL) analysis provides useful information on the existence and distribution of defects and trace elements in materials, which are related to genetic conditions such as formation temperature, metamorphic process and geochronological situation. U-Pb zircon dating (e.g., SHRIMP) is an important tool to determine geological age of a micro-ordered zircon, where CL image has been used for observation of internal zones and domains with different chemical compositions and structural disorder at spatial high resolution. CL of zircon is caused by various types of emission centers, which are divided into two groups: extrinsic center such as rare earth element (REE) and intrinsic center such as lattice defects. Above all, CL of zircon is closely related to metamorphic process and radiation from contained radionuclides. Most zircon has yellow emission, which seems to be assigned to radiation-induced defect or UO_2 centers. According to Nasdala et al. (2002) and Hancher and Hoskin (2003), the yellow emission band has been recognized to be eliminated by heat treatment. Therefore, the radiation effects on zircon CL have been studied for He^+ ion-implanted samples annealed at various temperatures to clarify radiation-induced defect centers involved with yellow CL emission in zircon.

A single crystal of zircon from Malawi (MZ) was selected for annealing and He^+ ion implantation experiments. The sliced samples were cut perpendicular to c- and a- axes, and annealed at 100 to 1400 deg. C for 12 hours. Zircon crystals in Takidani granodiorite (TZ) and Kurobegawa granite (KZ), and the sliced MZ were implanted by He^+ ion at 4.0 MeV corresponding to energy of alpha particle form ^{238}U and ^{232}Th. The radiation dose was set at 4.77 x 10^{-4} and 5.11 x 10^{-5} C/cm^2. CL spectra in the range from 300 to 800 nm with 1 nm step were measured by a scanning electron microscopy-cathodoluminescence (SEM-CL). The operating condition was set at 15 kV accelerating voltage and 0.1 nA beam current. All CL spectra were corrected for the total instrumental response.

CL spectra of untreated and annealed zircon almost show emission bands at ~370 nm assigned to intrinsic defect center and at ~480, ~580 and ~760 nm to Dy^{3+} impurity centers [Cesbron et al, 1995; Gaft et al, 2005]. Yellow CL emissions have been undetected in annealing zircons above 700 deg. C, where an elimination of radiation-induced defect centers may be appeared due to recrystallization of the structure suggested by Nasdala et al (2002). Blue CL intensity at ~370 nm gradually increases with an increase in annealing temperature, which may be responsible for a formation of intrinsic defect center due to a recovery of the framework structure from metamict by heating. CL spectra of MZ show an increase in the yellow emission intensity with an increase in radiation dose of He^+ ion implantation as well as the emission related to the impurity centers (REE), though He^+ ion implantation reduces the intensity of impurity centers. Yellow emission intensity has a tendency to depend on radiation dose of He^+ ion implantation. TZ and KZ, with young formation ages of 1.93-1.20 Ma and 1.7-0.9 Ma, respectively [Harayama,1994; Harayama et al., 2010], show dull yellow CL emission attributed to radiation-induced defect center, suggesting relatively low radiation dose of alpha radiation from ^{238}U and ^{232}Th on them. If the component of yellow emission could be deconvoluted from the CL spectra in zircon, the intensity of yellow emission should be used for an indicator to evaluate total exposure doses on it during geological age.

Keywords: Cathodoluminescence, Zircon, annnealing effect, radiation effect

SMP44-P11   Room:Convention Hall   Time:May 20 18:15-19:30

Emission mechanism of cathodoluminescence in smithsonite

Masato Makio[1]*, Hirotsugu Nishido[1], Nobuhiro Kusano[1], Kiyotaka Ninagawa[1]

[1]Okayama Univ. Sci.

Cathodoluminescence (CL) has been widely applied in mineralogical investigation, especially for carbonates. CL of carbonates is characterized by various types of emission centers such as impurity and defect centers. Smithsonite ($ZnCO_3$) has emission centers of divalent Mn ion as activator and divalent Fe ion as quencher (Gotte and Richter, 2004). However, the defect center in smithsonite has not been investigated so far, since its emission is not so often found in carbonates. We have detected blue CL emission in smithsonite, suggesting structural defect center. In this study, we have assigned emission bands in CL spectra including defect center and clarified the mechanism of the CL in smithsonite in a wide temperature range.

Three crystals of smithsonite from San Antonio, Mexico (S-08, S-11) and Slaiman, Uzbekistan (S-17) were selected for CL measurements after carbon-coating on their polished surfaces. SEM-CL analysis was conducted using an SEM (JEOL: JSM-5410) combined with a grating monochromator (Oxford: Mono CL2) to measure CL spectra ranging from 300 to 800 nm in 1 nm steps at accelerating voltage of 15 kV and beam current of 1.0 nA. The CL emitted from the samples was collected by a photon counting method with a photomultiplier tube, and converted to digital data. All spectra were corrected for total instrumental response determined using a calibrated standard lamp. The sample temperature can be controlled in the range from -190 to 50 degree C with flowing liquid nitrogen and using an embedded heater in a cryostage (Oxford: C1003). CL color imaging was carried out with Luminoscope (ELM-3 R) consisting a cooled CCD camera by excitation voltage at10kV and beam current of 0.5 mA.

CL spectra of S-11 at room temperature show a board band at around 650 nm in red region, which can be assigned to the electronic transition from excited state of 4G to ground state of 6S corresponding to divalent Mn activator substituted for Zn ion. S-08 has a broad band at around 400 nm in blue region in its CL spectrum. Its emission might be caused by the defect center in smithsonite lattice. S-17 has also emission peaks at around 650nm in red region and 400nm in blue region. The deconvolution of the spectra in an energy unit using a Gaussian fit reveals that a red emission has two components peaked at 1.61 and 1.82 eV and a blue emission consists of two components at 3.28 and 3.82 eV. Therefore, there are at least two deferent defect centers in smithsonite, suggesting different crystal fields between them. The intensity of a blue emission decreases with an increase of sample temperature as explained by a temperature quenching theory based on an increase in the probability of non-radiative transition with the rise of temperature (Mott-Seitz model). Activation energy in each temperature quenching process can be calculated by an Arrhenius plot using integrated intensity of each component as a luminescent efficiency. It results in activation energy of 0.027 eV for component centered at 3.28 eV. This energy value corresponds to the energy of O-Zn-O bending vibration (0.024 eV: Frost et al, 2008), suggesting energy-transfer from the radiation to lattice vibration as photon. However, the intensity of a red emission is not affected by the change of sample temperature. These facts indicate that the temperature quenching mechanism might depend on the types of emission centers related to impurity or structural defect.

Keywords: smithsonite, cathodoluminescence, emission mechanism

Numerical definition of particle size and shape of volcanic ash by statistical particle image analysis method.

Daisuke Sasakura[1*], HAYAUCHI Aiko[1]

[1]Malvern Japan ,Div of Spectris Co.Ltd,.

[1] Introduction

The exact definition of particle size and shape is a factor of importance in many researches connected with several geology sciences which objections are sea sand, soil and volcanic ash. The object of this report is to describe the various methods of defining these properties and to give the result of some measurements made on volcanic ash as model sample by statistical particle image analysis.

[2] Methodology

The statistical particle image analysis is possible to obtain the significant difference evaluated result of particle size and shape information by over the ten thousand numbers of particles projection images from microscopic method. The methodology of this technique is based on the digital binary image processing technology from projection image picture of CCD camera on microscope. In each CCD camera pixels has size. The determinations of particle size and shape parameter are calculated by the particle projection images which are constructed from the number pixels in CCD camera. The most of the advantage of this method is not only possible to described numerical definition of particle analysis but also available to the diverse analysis by two dimensional correlations plot between shape parameter and particle size.

[3] Material and method

Volcanic ash sample was from the Ito Pyroclastic Flow as model sample. This sample was sieved by 5 phi mesh sieve and it was come from under the mesh to isolate small particle from bulk sample. An automated particle characterization system (Morphologi G3,Malvern Instruments) was used to evaluation of statistical particle image analysis. The observation mode was diascopic mode (Transmittance mode) . Volcanic ash sample were dry dispersed using the integrated Dry sample dispersion unit via an instantaneous pulse of compressed air, and measured using Standard Operating Procedures (SOPs) which define the software and hardware settings depending. Measurements were made in an enclosed glass plate as sample carrier, minimizing environmental exposure. The analysis generated high quality images from over ten thousands of sample particles.

[4] Result

Total number of 96,029 particles was measured. Volume based circle equivalent diameter of particle size distribution (VCED) were monomodal and 14.31(d10), 30.32(d50), 45.79(d90) in micro meter. However, the number based percentage of small particles ($<$3 micrometer) was 74.91%. To concerning shape distribution and shown in Fig.1. Circularity was bimodal, however aspect ratio was monomodal. Recalculation of VCED was shown Fig.2 which was shape distribution data. Represented on amount of volume based percentage , the circle like particles were 3% and the angular like particles were 64% .However , in count based percentage , circle like particles were 55% and angular like particles were 21%.

[5] Summary

This report will be more discuss about application and capability of numerical definition of volcanic ash by the statistical particle image analysis as new approach for this research area.

Keywords: Volcanic Ash, Pariticle size, Pariticle shape, Particle Image Analysys
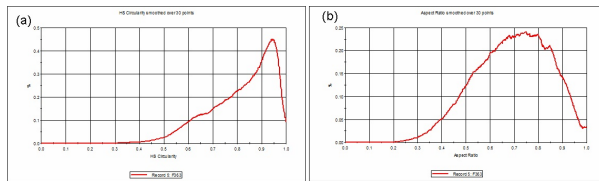
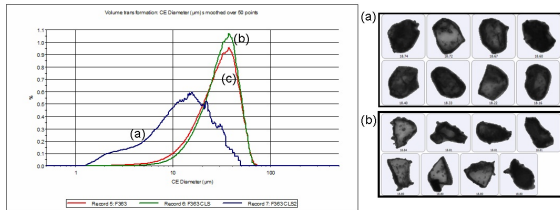Fig.1 Shape distribution by particle image (a) Circularity (b) Aspect ratio

Fig.2 Recalculated VCED (a) Circle like (Circularity >= 0.850 Aspect Ratio >= 0.450) (b) Angular like (Circularity Between 0.400 - 0.750 , Aspect Ratio >= 0.450) (c) Total

SMP44-P13	Room:Convention Hall	Time:May 20 18:15-19:30

Temperature quenching mechanism of cathodoluminescence in dolomite

Nobuhiro Kusano[1]*, Hirotsugu Nishido[1], Masato Makio[1], Kiyotaka Ninagawa[1]

[1]Okayama University of Science

Cathodoluminescence (CL) has been widely applied in mineralogical and petrological investigations, especially for carbonates. Dolomite commonly red CL emission related to an impurity center of divalent Mn (Reeder , 1987; Gillhaus et al, 2001), but of which each occupancy in Ca site (A site) and/or Mg site (B site) has not been precisely estimated. Furthermore, temperature effect on CL efficiency has not been discussed in spite of potentially important function to control CL emission mechanism, though the factors effected on dolomite CL such as luminescence centers have been extensively investigated. In this study we have clarified luminescent mechanism of dolomite in a wide range of temperature using a SEM-CL, and confirmed a temperature quenching of its emissions. The quenching process has been quantitatively evaluated by CL spectral deconvolution method assuming the Mott-Seitz model, where site occupancy for Mn^{2+} ions in dolomite lattice has been also evaluated.

Three dolomite samples from Binntal/VS, Swiss (D-17a), Arizona, USA (D-26a) and New Mexico, USA (D-28a) were selected for CL measurements after carbon-coating on their polished surfaces. These samples contain Mn^{2+} ions as an activator, but too low for divalent Fe as a quencher.

SEM-CL analysis was conducted using an SEM (JEOL:JSM-5410) combined with a grating monochromator (Oxford: Mono CL2) to measure CL spectra ranging from 300 to 800 nm in 1 nm steps with a temperature controlled stage from -190 to 250 ^{o}C . The dispersed CL was collected by a photon counting method using a photomultiplier tube (R2228) and converted to digital data. All CL spectra were corrected for the total instrumental response.

All samples exhibit a broad band in red region CL spectrum between 580 and 640 nm at room temperature. The spectral peaks are sharpened and enhanced at lower temperature due to reduction of thermal lattice vibration and an increase in luminescent efficiency, suggesting high spectral resolution of the emission bands at low temperature. Therefore, a Gaussian fitting was conducted to quantitatively deconvolute spectral data obtained at low temperature in an energy unit. Two emission components at around 1.84 and 2.15 eV. The former can be assigned to the emission derived from Mn ion impurity occupied at A site, the latter to the emission at B site. The component intensities decrease in two steps of temperature range between -190 to -100 and -50 to 150 ^{o}C with an increase in sample temperature. In general, luminescence efficiency of the material decreases with a rise in temperature due to an increase in non-radiative transitions. This phenomenon has been recognized in several minerals such as quartz, cristobalite and tridymite as temperature quenching. By assuming the Mott-Seitz model, activation energy in temperature quenching process can be calculated by a Arrhenius plot using integrated intensity of each component as an emission efficiency. Each activation energy was determined as follows; 0.03 eV for A and B sites below -100 ^{o}C and 0.100 eV for A site and 0.097 eV for B site above -50 ^{o}C. The former corresponds to the value of CO_3 vibration, and the latter to Ca-O or Mg-O vibration. Judging from the similarity of the activation energy in the process of temperature quenching and lattice vibration energy, the temperature quenching energy might be transferred as a phonon to the specific lattice vibration through non-radiative transition.

Keywords: dolomite, cathodoluminescence, temperature quenching